Accepted Manuscript

Title: Adsorption of bovine serum albumin on amorphous carbon surfaces studied with dip pen nanolithography

Authors: Pradeep K. Yadav, Fiona McKavanagh, Paul Maguire, Patrick Lemoine

Please cite this article as: P.K. Yadav, F. McKavanagh, P. Maguire, P. Lemoine, Adsorption of bovine serum albumin on amorphous carbon surfaces studied with dip pen nanolithography, *Applied Surface Science* (2010), doi:10.1016/j.apsusc.2011.08.068

This is a PDF file of an unedited manuscript that has been accepted for publication. As a service to our customers we are providing this early version of the manuscript. The manuscript will undergo copyediting, typesetting, and review of the resulting proof before it is published in its final form. Please note that during the production process errors may be discovered which could affect the content, and all legal disclaimers that apply to the journal pertain.

Adsorption of bovine serum albumin on amorphous carbon surfaces studied with dip pen nanolithography

Pradeep K. Yadav, Fiona McKavanagh, Paul Maguire, and Patrick Lemoine*

Nanotechnology and Integrated BioEngineering Center, University of Ulster at Jordanstown, Shore road, Newtownabbey BT37 0QB United Kingdom

*To whom correspondence should be addressed. Tel: +44 (0)2890368054; Fax: +44 (0)2890366863;

E-mail: p.lemoine@ulster.ac.uk

Abstract

This article reports the use of dip pen nanolithography (DPN) for the study of adsorption of bovine serum albumin (BSA) proteins on amorphous carbon surfaces; tetrahedral amorphous carbon (t-aC) and silicon doped hydrogenated amorphous carbon (a-C:H:Si). Contact angle study shows that the BSA proteins reduce the contact angle on both carbon materials. We also noticed that the drop volume dependence is consistent with a negative line tension; i.e. due to an attractive protein/surface interaction. The DPN technique was used to write short-spaced (100 nm) BSA line patterns on both samples. We found a line merging effect, stronger in the case of the a-C:H:Si material. We discuss possible contributions from tip blunting, scratching, cross-talk between lever torsion and bending and nano-shaving of the patterns. We conclude that the observed effect is caused in large measure by the diffusion of BSA proteins on the amorphous carbon surfaces. This interpretation of the result is consistent with the contact angle data and AFM force curve analysis indicating larger tip/surface adhesion and spreading for the a-C:H:Si material. We conclude by discussing the advantages and limitations of DPN lithography to study biomolecular adsorption in nanoscale wetting environments.

Keyword: DPN, BSA, Contact angle, LFM.

Adsorption of bovine serum albumin on amorphous carbon surfaces studied with dip pen nanolithography

Pradeep K. Yadav, Fiona McKavanagh, Paul Maguire, and Patrick Lemoine*

Nanotechnology and Integrated BioEngineering Center, University of Ulster at Jordanstown, Shore road, Newtownabbey BT37 0QB United Kingdom

*To whom correspondence should be addressed. Tel: +44 (0)2890368054; Fax: +44 (0)2890366863;

E-mail: p.lemoine@ulster.ac.uk

Abstract

This article reports the use of dip pen nanolithography (DPN) for the study of adsorption of bovine serum albumin (BSA) proteins on amorphous carbon surfaces; tetrahedral amorphous carbon (t-aC) and silicon doped hydrogenated amorphous carbon (a-C:H:Si). Contact angle study shows that the BSA proteins reduce the contact angle on both carbon materials. We also noticed that the drop volume dependence is consistent with a negative line tension; i.e. due to an attractive protein/surface interaction. The DPN technique was used to write short-spaced (100 nm) BSA line patterns on both samples. We found a line merging effect, stronger in the case of the a-C:H:Si material. We discuss possible contributions from tip blunting, scratching, cross-talk between lever torsion and bending and nano-shaving of the patterns. We conclude that the observed effect is caused in large measure by the diffusion of BSA proteins on the amorphous carbon surfaces. This interpretation of the result is consistent with the contact angle data and AFM force curve analysis indicating larger tip/surface adhesion and spreading for the a-C:H:Si material. We conclude by discussing the advantages and limitations of DPN lithography to study biomolecular adsorption in nanoscale wetting environments.

Keyword: DPN, BSA, Contact angle, LFM.

1. Introduction

The understanding and control of protein interactions with material surfaces is key to two broad health-related issues;-i) the development of viable biomedical implants and –ii) the toxicity of nanomaterials. For most implant situations, the implantable material will be adequate if it can favour/inhibit specific cell adhesion pathways, which in turn are often switched on by the release of specific proteins. Hence the biocompatibility of the implant material is in large measure dependent on how proteins adsorb on its surface. For example, the haemocompatibility of a surface is often enhanced by low fibrinogen adsorption and/or high human serum albumin (HSA) adsorption as the former is a precursor to the formation of fibrils and the anchoring of blood platelets. The toxicity of nanomaterials is also in large measure dependent on protein adsorption. Here again, the foreign substance interacts with the biological medium through its surface and principally through protein adsorption. If this result in protein misfolding especially desorbed misfolded proteins, it can be followed by a change in the protein function and toxicity. Finally, protein condensation diseases such as arthritis, cataract, Alzheimer, Parkinson and Prion diseases are also examples of protein misfolding creating biological havoc.

Hence, protein adsorption is of interest to many but despite an intense research effort and a large range of investigations, some challenges remain, mainly due to the large number of proteins concerned, even for relatively focused problems (i.e. haemocompatibility). One difficulty is that proteins are small, data from X-ray crystallography show typical dimensions of a few nm [1]. Many protein adsorption studies have shown that an essential perquisite of this type of investigation is to work with ultra-smooth surfaces, typically $R_a < 1$ nm. As most medical grade materials are much rougher [2], fundamental investigations of

1

this nature must be completed firstly on model surfaces to differentiate the effect of topography and surface composition on the protein behaviour [3]. Another challenge is that investigations of the adsorption or misfolding of proteins require detection methods with great surface sensitivity and good spatial resolution. Finally, an established technique to probe biomolecular adsorption behaviour is to use fluorescent labels. This method is well suited to relatively short biomolecules, like single strand DNA in the sense that the adsorption site and tag are in well defined positions at opposite ends of the molecule. With proteins, one can never be sure that the tag will not interfere with the rich and complex secondary structure of the protein and therefore with the adsorption process [4].

In this work, these challenges are addressed by taking novel approaches; -i) using amorphous carbon as a model protein adsorption surface as it is an ultra-smooth, amorphous, mono-elemental material with biocompatible properties [5] and –ii) studying the protein adsorption with a tag-less detection technique with nanoscale spatial resolution; dip pen lithography (DPN).

We focused this investigation on bovine serum albumin (BSA), a non-specific globular protein which is generally used for its stability, lack of effect in many biochemical reactions, low cost and abundant supply. More specifically, BSA bear many resemblances with Human serum albumin (HSA), the main protein contained in blood plasma, it can help the non-specific binding of hydrophobic steroids, it is used in immunodiagnostic procedures (ELISA), as a clinical chemistry reagent, as a nutrient for cell culture media and finally, BSA can also be used to determine the amount of other proteins [6].

To date, the adsorption of protein on hydrophobic and hydrophilic surfaces has been studied extensively, for instance with AFM, XPS, FTIR, and optical waveguide light mode spectroscopy [7], however, there has been no specific adsorption study either using DPN lithography on amorphous carbon surfaces.

2. Experimental

In this study, the BSA proteins were 66 KDa obtained from Sigma-Aldrich, in dried powder form. The BSA ink solution was an aqueous suspension prepared with distilled water with a BSA concentration of 1 mg/ml. In contact with atmosphere, DI water is usually at pH 7, a condition where BSA is usually in its native conformation [8]. The amorphous carbon films used in this work were of two types, tetrahedral amorphous carbon (t-aC), a hard (40-70 GPa hardness) and insulating carbon material, mainly sp^3 carbon prepared by filtered vacuum cathodic arc deposition (FCVA) and a silicon doped hydrogenated amorphous carbon (a-C:H:Si), a softer (10-20 GPa hardness) deposited by plasma enhanced chemical vapour deposition (PECVD). These films are regularly produced in our laboratory and have been extensively characterised [9-10]. The Si doping is used to decrease the roughness of the a-C:H film, nonetheless, the t-aC material is smoother again. Tapping mode Atomic force microscopy (TAFM) images were obtained with a Veeco DI3100 SPM system using TESP levers (nominal stiffness ~ 40N/m) operated slightly below resonance (~300 kHz) with high set point amplitude (~80% amplitude with respect to the free amplitude measured 500 nm above the surface; hydrodynamic damping is taken into account). The R_a roughness values for 1 μm TAFM scans are 0.4 nm and 1 nm for the t-aC and a-C:H:Si materials , respectively.

The DPN system in use here was from NanoInk Inc. It uses a Pacific Instruments AFM microscope and a series of ink wells useful for dispensing the ink onto the AFM tip. The inking can be done by AFM approach or manually. Generally, we adopted the double dipping procedure [11], consisting of ink dipping, drying, DI water dipping, drying and again ink dipping. The software of the instrument allows to-link the optical micrographs to the positioning control so that the DPN process can be applied to the desired substrate region. All the DPN patterning experiments had been done by NanoInk's InkCAD version 3.6.2 NSCRIPTOR system and with controlled environmental conditions (relative humidity 30±1% and temperature of 22±1 ^{0}C). Unless specified otherwise, the AFM system was operated in contact mode using either silicon nitride single array DPN probes (nominal stiffness ~ 0.1 N/m) or the TESP Si probes. The spring constants were calibrated using the resonant frequency, Q factor and lever width and length, using the Sader method [12]. The cantilever deflection sensitivity was calculated using a force curve on a hard and smooth sapphire substrate. The DPN writing was done in CAFM mode at low scanning speed (typically 0.6 μm/s) while imaging was carried out LFM mode at higher speed (~9 μm/s). The working hypothesis, also adopted in other DPN

2

studies [13], is that the difference in speed insures minimal writing or erasing during the imaging process while the LFM mode permits to detect ink features with small topographic contrast. However, the validity of this assumption will be discussed with the results.

For both AFM systems, the geometry of the probes was monitored using a blind reconstruction algorithm [14] (SPIP software) on Nioprobe standards (Electron Microscopy Sciences). Finally, the wettability of these carbon surfaces was measured using a sessile drop contact angle system (CAM 200 from KSV Instruments Ltd) with, typically, microliter volumes. Saving the optical micrographs of the sessile drops also allowed to calculate the drop radius, which was used for studying line tension effects for small drop volumes.

3. Results

Figure 1 shows the dependence of contact angle on drop volume for a solution of BSA protein and water on t-aC and a-C:H:Si surfaces. It shows that, for both substrates and for the two liquids, the contact angle decreases at small drop volume, this trend being stronger for water for both t-aC and a-C:H:Si. Also, the θ values for water are higher.

Using the TESP levers, BSA protein lines were written once (0.6 μm/s) with short spacing (100 nm) and subsequently imaged (9 μm/s) at various time interval (0 min to 300 mins every 30 min, figure 2) to study the evolution of protein-protein and protein-surface interactions. After about 90 mins, the lines are merging; i.e. they fuse together. This can be shown clearly on the cross-sections presented in the insert of figure 2.

The topographic images were much more difficult to obtain as the measured heights were small (smooth t-aC surface and very 'thin' ink layer). An example is shown in figure 3. The height are sub-nm but one can clearly see that, here again, the lines are merging. One note, however, that these are negative heights (dark contrast). Statistical analysis from the cross-sections gives line depths of 0.67 ± 0.33 nm at 0 min and 0.33 ± 0.13 nm at 300 min for the short-spaced lines (fig. 3a and 3b).

The DPN line merging observed in figure 2 is displayed in figure 4 as a change in LFM contrast. This was calculated using the LFM cross-sections, such as shown in the insert of figure 2, as the average peak-to-valley amplitude for adjacent lines, averaged over the seven lines. Clearly, this signal decreases with time. On the same figure, we display the same data for the a-C:H:Si sample. Clearly LFM contrast is a relative quantity and nothing can be said about the magnitude of this signal for the two materials. However, comparing the two carbon surfaces, one can see that the change in LFM contrast occurs earlier and is more abrupt for the a-C:H:Si surface.

Finally, we transferred the BSA dipped tips to the Veeco DI3100 AFM to obtain force distance measurements with better force resolution (~1 nN). The results, averaged over ten force curves, are shown in figure 5 and 6. The oscillations before approach are due to laser light interferences. The attractive force (F_1) and adhesion force (F_2) are larger for the a-C:H:Si material.

The short-spaced DPN lines were written with stiff TESP Si probes at relatively high forces (~ 6 μN). Figure 7 shows images taken with these same BSA-dipped tip on a Nioprobe standard sample before (0 min) and after (300 min) writing the short-spaced DPB lines. The nanostructure of the sample is finer for the image acquired before writing. The corresponding radius values for the tip X and Y profiles were determined using the SPIP software. The program fits a cone with a spherical cap to 3D shape obtained by blind reconstruction. This model only fitted over a 42 nm lateral range, a sufficiently large window considering the small surface features measured here. The determined radii in the two directions were R_x=101 ± 10 nm and R_y=89 ± 10 nm for the image acquired at 0 min and R_x=207 ± 10 nm and R_y=307 ± 10 nm for the image acquired at 300 min, the tip profiles (data and fit) are shown in the inserts of figure 7. The AFM tip, fairly blunt because of the high force is getting blunter, and more so in the Y direction which is the scanning direction for the LFM acquisition mode.

Finally, non-interacting DPN lines were written with larger spacing, ~300 nm and 1000nm, using in this case a soft Si_3N_4 lever with a lower force set point (~15 nN). The LFM lines are shown in figure 8 for the t-aC and

3

a-C:H:Si materials, respectively. For the a-C:H:Si surface, the lines are much wider; 185 nm for a-C:H:Si and 75 nm for taC. We also observed that the width of the lines written on the t-aC surface decreases with time; 75 nm at 0 min, 52 nm at 30 min and 33 nm at 48 hours. A similar effect was observed for the lines observed in height mode (figure 3c and 3d). For these large spacing experiments, the blind tip reconstruction of the tip gave Ry=17 nm, suggesting in this case no interaction between the lines.

4. Discussion

Generally, proteins are designed by nature to be water soluble, so as not to aggregate. For most proteins, this is accomplished by having buried hydrophobic groups to avoid the entropically-driven hydrophobic attractive interaction. In addition, there are often negatively charged groups on the outer surface which further inhibit the clustering and aggregation. Once in contact with the surface, the interactions between surface groups or even buried ones may be strong enough to change the protein conformation. In that regard, the above results show a number of interesting effects which may be evidence of conformational changes.

Figure 1 indicates that the contact angle of water on t-aC is between 60° and 75°, in line with previous literature studies, this is due to its low surface energy, according to previous studies ~25-40 mN/m fairly dispersive in nature, making it not very wettable [15-16]. BSA lowers the contact angle of water on t-aC. This could indicate that t-aC interacts more favourably with BSA proteins than with water molecules. Electrical attraction is unlikely as proteins such as BSA often have negative groups on their surfaces [17] and t-aC has a low electron affinity. A more plausible mechanism is the hydrophobic interaction which entropically chasses water molecules away from the t-aC surface and hence bring the proteins in contact with the surface. In that regard, the complexity and structural flexibility of BSA may result in chemical groups with more affinity to t-aC. Finally, proteins can act as surfactants; albumin is known to reduce the surface tension of water [18] which quite independently from the BSA/t-aC interactions would decrease the contact angle.

Figure 1 shows similar trends for the a-C:H:Si material and qualitatively, the same comments could be made about the interaction of water or BSA solutions with this amorphous carbon. Comparing the two materials one notices that, first of all, a-C:H:Si has higher θ values than t-aC. In the literature, aCH is often more wettable than t-aC but Si doping of aCH is known to increase the contact angle on water [19]. We also notice that the decrease in contact angle between water and the BSA solution are larger for the a-C:H:Si film than for the t-aC film ($\Delta\theta$= 15⁰ and 5⁰ for a-C:H:Si and t-aC, respectively, extrapolated at 0 μl). We recall that θ is defined from the Young-Dupre equation by;

$$\cos\theta = \frac{(\gamma_{SV} - \gamma_{SL})}{\gamma_{LV}}$$
(1)

Where γ_{SV}, γ_{SL} and γ_{LV} respectively represent the vapour-solid interfacial energy, the solid-liquid interfacial energy and the vapour-liquid surface tension.

Hence with $\Delta\gamma_{LV}$ being the same for the two carbon surfaces, the larger $\Delta\theta$ for the a-C:H:Si surface means that there is a larger change in (γ_{SV} γ-γ_{SL}). This would indicate, in turn that the BSA molecules have a larger affinity to the a-C:H:Si surface. This is also consistent with current results which emphasise the role of Si-doping in enhancing the adsorption of albumin with respect to that of fibrinogen [20].

The drop volume trends shown in figure 1 can be interpreted with the concept of line tension σ [21]. The surface tension γ_{AV}(called γ henceworth) represents the energy imbalance between water molecules on the

4

surface (two-phases boundary) and those immersed in the liquid bulk, as the surface is a gas/liquid boundary. Similarly, the water molecules at the contact line are at a three-phase boundary and therefore may well have different energetics than those present on the surface of the drop. This concept allow us to take into account the effect of drop radius with the following relationship;

$$\cos \theta = \cos \theta_\infty - \sigma / \gamma . R \qquad (2)$$

Line tensions measured in the literature are usually from 10^{-5} μJ/m to 10 μJ/m, although the higher values are usually attributed to the effect of surface roughness [18]. The sign of the line tension has also been hotly debated [18, 19, 26]. Some argue that σ can be positive or negative depending on the surface and liquid properties [22]. Others affirm, using equilibrium thermodynamics, that for the case of a smooth planar surface without heterogeneities, σ should always be positive, just as γ is always positive [18], one being an areal energy density while the other is a linear energy density. We note, however, that there is a more fundamental difference between surface tension and line tension. The positive sign of the surface tension γ corresponds to the excess energy that liquid molecules have on the drop surface, owing to its assymetry and the weak interactions with the adjacent medium, the gas; it takes energy to bring a water molecule from the core of the drop to its surface. This holds also for the surface energy of solid surfaces and both quantities are positive. On the other hand, the line tension represents a three phase boundary, so is also influenced by the interaction between the two condensed phases; the liquid and the solid. Again, a positive sign corresponds to an excess of energy or a repulsive interaction whereas a negative sign indicates an attraction or adhesion process. For the interfacial energy γ_{sl}, the wide range of affinities between solids and liquids means that this quantity can be either positive or negative. Likewise, the sign of the line tension σ may also change.

The drop volume dependence of the contact angle and the fit to equation 2 are presented in figure 9 and show the line tension effect to be minimal for the BSA solution but larger for water. Taking surface tension values of 72 mN/m for water and 50 mN/m for the BSA solution [17], we calculated line tensions of -15 μJ/m for the BSA/t-aC and -57.6 μJ/m for water/t-aC. Fitting the a-C:H:Si data gave similar values. This would seem to indicate that, as the drop volume decreases, BSA molecules do not migrate to the contact line to the same extend than water molecules, for both t-aC and a-C:H:Si substrates. It may be argued that, with respect to the center of the solid/liquid area where water molecules can only interact with the surface, the contact line represents a more favourable location as the water molecules can points their oxygen atoms towards the air region. In the literature, line tension effects have been discussed for contact angle experiments (μL to mL regime) but not for AFM studies (aL regime). This is surprising as the singularity of the contact line is bound to increase at the smaller scale, this nanoscale wetting phenomena being obviously relevant to DPN lithography.

The DPN results for the short-spaced lines indicate a modification of the LFM line pattern with time for both the t-aC and a-C:H:Si materials. This result could be due to re-deposition of ink during the imaging process. However, figure 3 indicates that after 8 images (300 min), there was no cumulative increase of the topographic feature, hence, if the BSA ink is deposited, it is only during the first 'inking' (0.6 μm/s) at 0 min and not during the subsequent imaging steps. To check whether BSA ink was indeed deposited, we used a dry tip (no BSA dipping) and performed the same experiment (ie TESP tip of equivalent radius with the same loading conditions). The results are shown in figure 10. There is an LFM signal, possibly due to removal of surface contamination, however, this pattern is quickly removed by the consecutive AFM images. By contrast, the LFM patterns obtained for BSA-dipped AFM tips on taC are stable up to 11 images and 48 hours. It is therefore likely that these correspond to adsorbed proteins.

The line merging effect observed for the short spaced DPN lines could be due to a number of processes. Firstly the AFM tip may disturb/ re-collect the adsorbed proteins. However, this nano-shaving effect would also occur on large spaced DPN lines, which we do not observe. Hence, we believe that this nano-shaving is not the major contributor to the observed line merging effect.

5

Another important consideration is the tip blunting occurring during inking/imaging and yielding to an incomplete reading of the surface, ie a line merging effect. For a given R_y tip radius, the smallest surface curvature x than one can observe for a depth y is;

$$X = (2R_y - y^2)^{1/2} \qquad\qquad (3)$$

Looking at the short spaced BSA lines obtained at, respectively, 0 min (R_y=89 nm y_{max}=0.67 nm) and 300 min (R_y=307 nm, y_{max}=0.33 nm), we find x values of 11 nm and 14 nm. We reproduce in figure 11, the 0 min surface Y profile, extracted from figure 3a and 3b with the corresponding tip Y profiles superimposed on the graphs. Clearly, despite the broad tips, the features are so shallow that there are no obvious tip artefacts. At 0 min, the tip is capable of reading the profile. At 300 min, the surface features are down to the instrumental noise level, however this broader tip would still be able to image the somewhat larger 0 min surface features (see over imposed red 300 min tip profile on the 0 min surface profile). Hence, there are no tip convolution artefacts.

Height artefacts can also be caused by the LFM cross-talk as the bending axis of the lever is never perfectly aligned with the axis of the photodiode. In the present case, we measured a 82 mV bending signal (topography) for a 1V LFM signal. With a 50 nm/V deflection sensitivity, this gives a 0.41 nm height artefact for an LFM signal of 100 mV (i.e. typical for figure 2), hence a significant contribution to the measured heights. Indeed, having completed recently an investigation on a large variety of ink/surface systems [23], we note that DPN line heights can be negative or positive and that in all cases, the measured heights are small (sub-nm). We therefore believe that this LFM cross-talk contributes significantly to the height artefact. In addition to this, the lever torsion affects the bending stiffness of the lever. As LFM images are usually acquired with deflection feedback, this means that these images are not obtained under constant force set point.

Another point of interest is the surface feature height resulting from the short spaced DPN lines; -0.33 to -0.67 nm for taC, Firstly, these small negative height features can be caused by the interaction of the written lines through a pile-up mechanism [24]. However, the topographic CAFM images of figure 3c and 3d also show a negative height contrast. As these lines were written with large spacing (300 nm) and a small tip radius (~ 17 nm), they did not interact with one another. Hence this explanation is not plausible. Secondly, a small negative height may be due to scratching of the taC surface. Based on a normal load of 6 μN, a Young modulus of 420 GPa for the taC layer, obtained from previous nanoindentation measurements [25], contact mechanics theory gives deformations of 0.68 nm and 1.05 nm for the TESP tip at 0 min and 300 min, respectively. In these calculations, we used the Johnson-Kendall-Roberts theory [26] with adhesion forces measured from AFM force curves such as shown in figure 5. However these estimates do not take into account the influence of lateral forces on the deformation. Moreover the height images for the dry TESP tip (figure 10) show no scratching. In addition, the LFM cross-talk artefact already mentioned prevents a meaningful estimation of the height signal. This means that scratching of the carbon substrate cannot be completely ruled out, from theoretical calculations, but is difficult to prove experimentally.

Scratching and deformations may also affect the protein layer. In its native state, the BSA molecule is a prolate ellipsoid 4x4x14 nm [27]. Under the AFM tip, it may be compressed. Such an effect has been observed recently in a DPN study of the adsorption of BSA on mica surfaces, with measured protein heights of 0.5-1 nm [6]. Indeed, it is likely that such a soft protein with low structural integrity [6] may deform and possibly change conformation under the significant normal load. In this regard, it is informative to consider how the proteins may behave under the conditions of figure 2; i.e. large tip radius, and short spacings, with lines nearly 'touching'. Hence, through long range interactions, the BSA proteins from adjacent lines can interact with one another. However, to move across the surface requires favourable interactions with this surface. The fact that this happens more quickly for the a-C:H:Si material, would suggest stronger interaction with the BSA proteins in this case. The force curve data of figure 5 and 6 are consistent with this interpretation, the adhesive force F_2 is larger for the a-C:H:Si material (300 ± 23 nN for a-C:H:Si and 166 ± 10 nN for t-aC). This material also exhibits smaller x_1 and x_2 values, the meniscus formation height and final

6

heights, indicating that the stronger tip/surface attraction is also of shorter range. The meniscus capillary force F_2 can be calculated as;

$$F_2 = 4 . \Pi . R . \gamma . \cos (\theta) \qquad (4)$$

With a value of 50 mN/m for the surface tension of the BSA solution, we find that in the nanoscale liquid bridge, $\cos \theta \sim 1$ ($\theta \sim 0^o$) for a-C:H:Si and $\cos \theta \sim 0.58$ ($\theta \sim 54^o$) for t-aC. In other words, at the nanoscale, we get full wetting for a-C:H:Si and partial wetting for t-aC. The difference between macroscale and nanoscale wetting is consistent with the observed line tension effect, mentioned above. It can also result from the effect of protein concentration; in the AFM meniscus; the BSA solution being probably saturated (10 mg/ml) [28]. This implies a larger affinity of BSA to a-C:H:Si than to t-aC. It is also consistent with the observation that the $\Delta\theta$ from water to the BSA solution is larger for the a-C:H:Si material. These findings would mean that the BSA protein adopt different surface conformation once adsorbed on the a-C:H:Si and t-aC surfaces. The surface area of the protein can be estimated as follows. The line widths of the DPN lines at 0 min, 185 nm for a-C:H:Si and 75 nm for t-aC, correspond to the meniscus diameter d. The distance x_2, measured from the force curve (figure 7) gives the meniscus height before pull-off. In the present case (large h and R values), the meniscus volume can be modelled as a cylinder, i.e. $V = \pi . d^2 . x_2/4$. Again, assuming a saturated BSA solution in the meniscus and monolayer coverage, we can calculate the number of proteins in the adsorbed area $\pi . d^2/4$, hence the average surface area of the absorbed proteins. The result of these calculations is that the BSA molecules spread on 90 nm^2 on a-C:H:Si and 64 nm^2 on t-aC, whereas typical BSA cross-sectional areas in solution are 24-28 nm [26]. This means that the DPN process has resulted in unfolding and more so in the case of the a-C:H:Si material. One also notes that the nanoscale spreading of the meniscus discussed above is bound to accentuate this trend, although the validity of equation 4 for describing nanoscale liquid bridges has been challenged [29].

In any case, this larger affinity of a-C:H:Si to BSA could be due to its electronic structure. Hydrogenated amorphous carbons prepared by PECVD have a larger sp^2 fraction than t-aC materials prepared by FCVA. This result in smaller band gap but larger work function, in other words, larger electron affinity, which may result in easier adsorption for the BSA surface, usually covered of negative groups. Another factor is that the hydrogenated carbon surface favours attractive VDW interactions with BSA protein groups, especially buried hydrophobic groups, this potentially resulting in significant unfolding.

The above discussion is consistent with the DPN results obtained on t-aC for large spacings. The narrowing of the lines with time could be due to the aforementioned less favourable interactions between t-aC and BSA. Finally, at larger spacings, the lines written on a-C:H:Si were also broader than on t-aC (figure 8), again an indication that BSA proteins diffuse more readily onto the a-C:H:Si surface than on the t-aC one.

These results are preliminary but consistently point towards the same conclusion; i.e. BSA adsorbs more readily onto a-C:H:Si than on t-aC surfaces. This has implications for the use of these materials as biocompatible coatings for implant devices. For instance, thrombosis and blood clotting is triggered by the adsorption of fibrinogen into fibrin which itself paves the way for platelet adsorption. As these processes happen in competition with the adsorption of human serum albumin (HSA), a large HSA adsorption could be a good way to prevent clotting. HSA and BSA are not very different chemical entities; hence the results above might be of relevance to this important biomedical issue. Further work is required where the adsorption of both fibrinogen and HSA can be studied concurrently with DPN lithography.

Finally, this investigation also outlined the peculiarities of using DPN lithography to study protein adsorption. The techniques has obvious advantages; it permits to deposit proteins at specific sites, with nanoscale resolution and henceforth follow the kinetic of the adsorption process, it allows for tag-less detection of proteins, an important attribute considering the possible interference between the fluorescent labels and the adsorption process. There are also significant issues which must be considered. The nanoscale wetting behaviour is likely to differ from its macroscale counterpart because of line tension effects. The interaction between the AFM tip on the adsorbed ink must be closely monitored as a number

7

of effects can occur such as tip blunting, scratching and shaving of the ink/surface system and, finally, the LFM acquisition which represents the main mode of operation of the DPN technique can bring a number of artefacts in the case of soft adsorbates or small surface features.

5. Conclusion

We have studied how DPN can be used to study the adsorption of BSA proteins on amorphous carbon surfaces. BSA reduces the contact angle on both t-aC and a-C:H:Si materials but more so for the later material. We also observed drop volume dependence consistent with a negative line tension. Short-spaced BSA line patterns formed by DPN showed larger line merging for the a-C:H:Si film. We found that the effect was due to the surface diffusion of BSA molecules across the amorphous carbon surface, although other effects were also considered (tip blunting, scratching, LFM artefacts). This interpretation is consistent with AFM force curves; the a-C:H:Si material exhibits the larger adhesion force. By contrast, short-spaced t-aC patterns showed less line merging. For t-aC lines patterns with large spacing, we observed a narrowing of the lines, again consistent with less interaction of the BSA molecules with the t-aC surfaces. Initial calculations derived from DPN and AFM force curve data indicate that the BSA proteins spread more over the a-C:H:Si surface, a result consistent with the main experimental findings. The relevance of this initial study on the bio-implantability of amorphous carbon is discussed. Finally, we emphasise the specificity of nanoscale wetting behaviours and their relevance to DPN studies of biomolecular adsorption.

8

Figure Captions

Figure 1. Dependence of contact angle on drop volume. These measurements correspond to DI water and the BSA solution on t-aC and a-C:H:Si substrates.

Figure 2. 3.3 μm LFM images of short-spaced DPN line patterns of the BSA ink on a taC substrate at various time intervals. Two LFM cross-sections are also shown in the insert.

Figure 3. 3.3 μm Height AFM images (2nm vertical scale) of DPN line patterns on a taC surface, a/ short-spaced (100 nm spacing) 0 min, b/ short-spaced (100 nm spacing) 300 min, c/ large-spaced (300 nm spacing) 0 min and, d/ large-spaced (300 nm spacing) 300 min.

Figure 4. LFM contrast change versus time, for DPN writing of closely spaced lines on t-aC and a-C:H:Si surfaces.

Figure 5. AFM force curves obtained on t-aC (left) and a-C:H:Si (right) with the BSA-dipped tip used after writing closely spaced lines (100 nm spacing).

Figure 6. Bar chart of the adhesion forces and distances; averaged over 5 measurements.

Figure 7. 1 μm TAFM height scans (20 nm vertical scale) of Nioprobe standard samples obtained with the BSA-dipped TESP tips for 0 min and 300 min short spaced DPN writing. The inserts represent the corresponding tip Y-profiles extracted from the blind reconstruction, with the scales expressed in nm.

Figure 8. LFM images and cross-sections for large-spaced BSA DPN lines on t-aC (300 nm spacing) and a-C:H:Si (1000 nm spacing). The space bar represents 1 μm.

Figure 9. Fitting to equation 1, effect of drop volume/radius on line tension for the BSA/t-aC and water/t-aC systems (left); and for the BSA/a-CH and water/a-CH systems (right).

Figure 10. Height and friction profiles obtained with a dry TESP tip on a taC surface. In the center of the images is a small rectangle (1x0.5 μm^2) scanned slowly (0.6 μm/s) at high force (~6 μN), the images shown (2x1 μm^2) are scanned more rapidly (9 μm/s) at a lower force (~1 μN), a/ first, b/ second, c/third and d/ fourth consecutive images.

Figure 11. Y surface profiles (nm, nm) from the CAFM height image of the BSA DPN line pattern on taC for the 0 min conditions. The AFM tip Y profiles have been reproduced to scale for the 0 min (black) and 300 min (red) conditions.
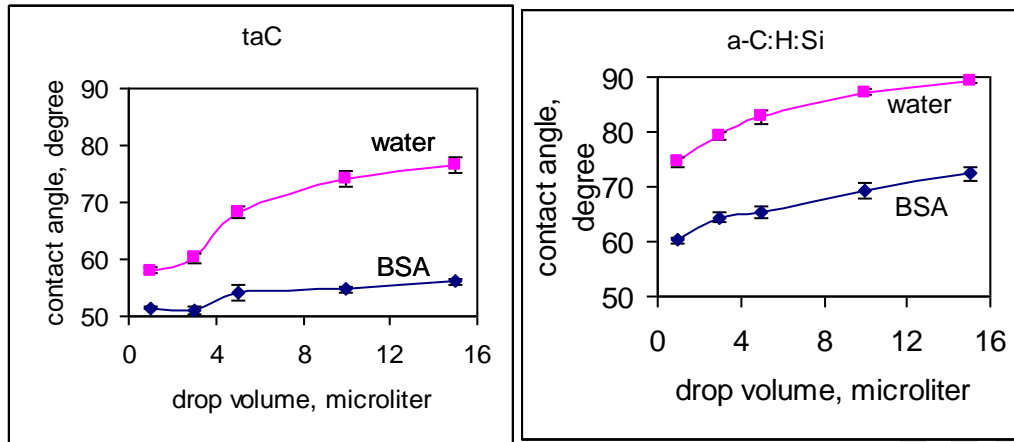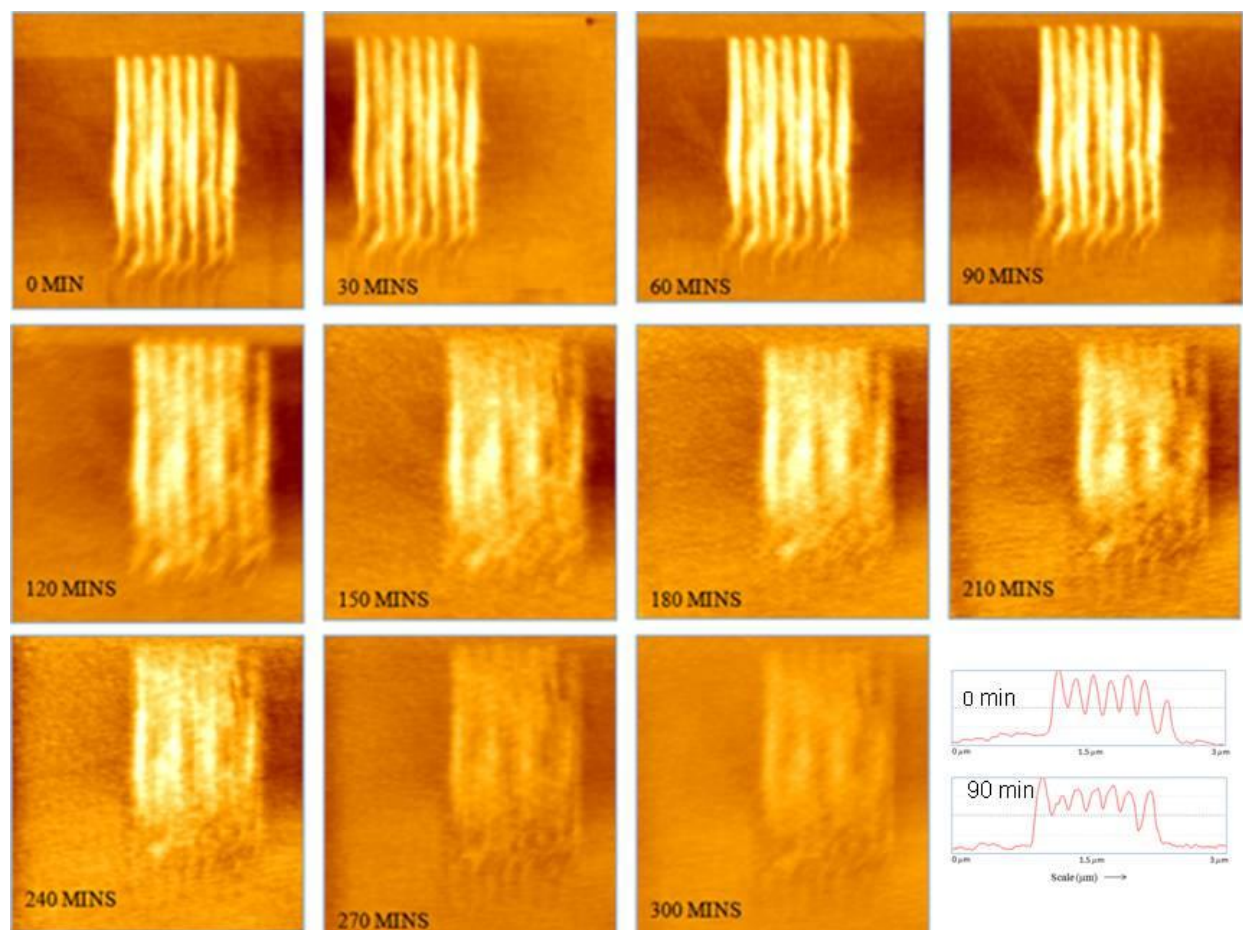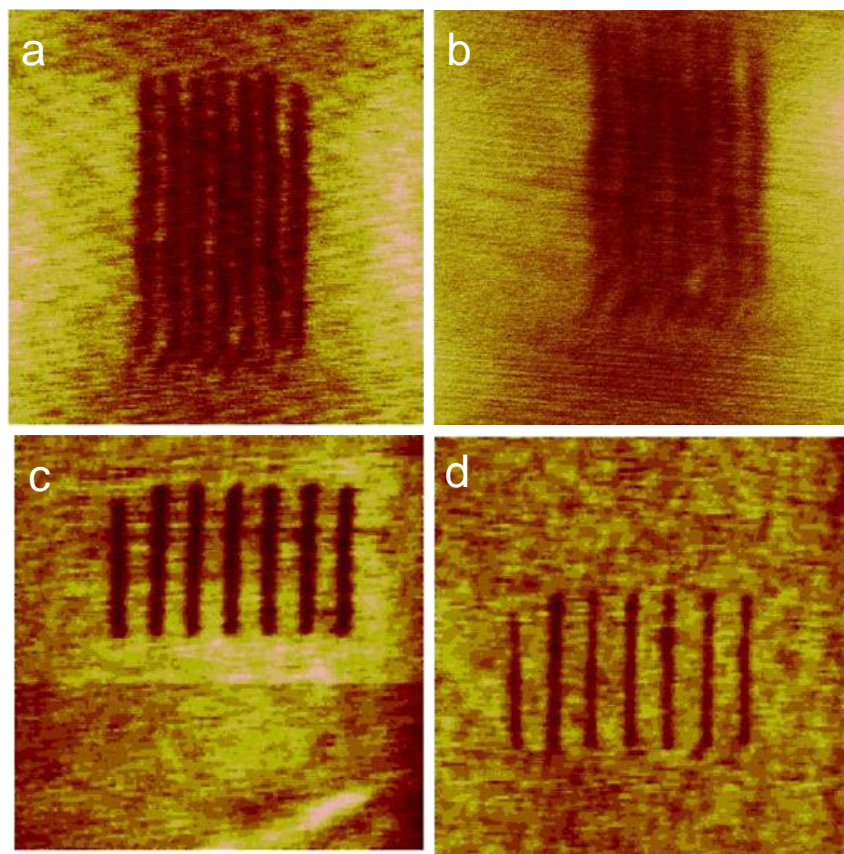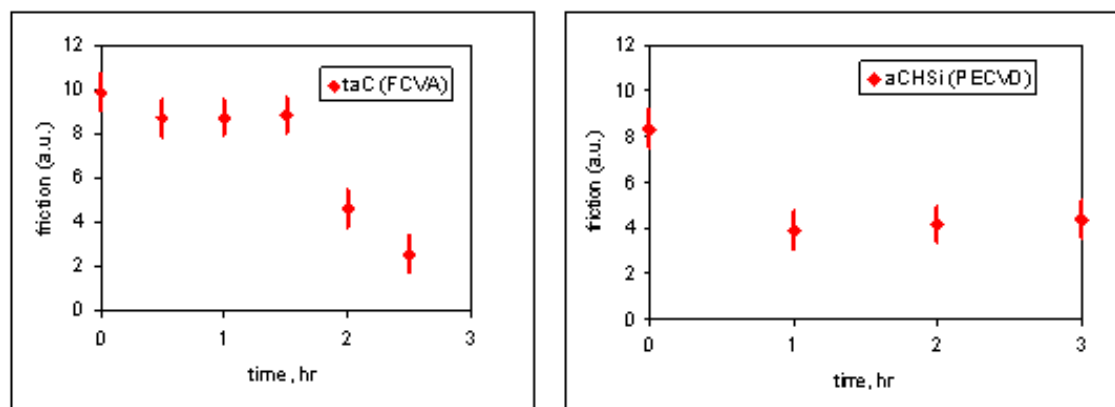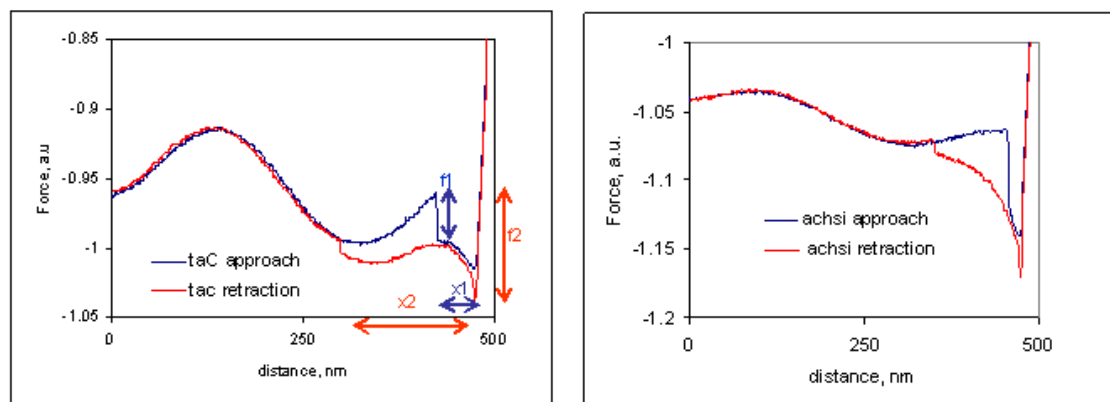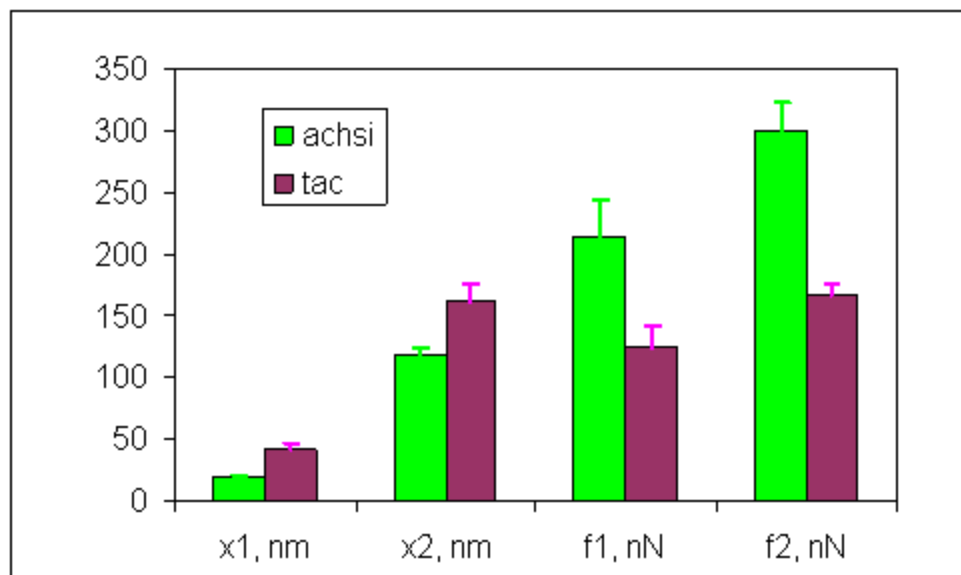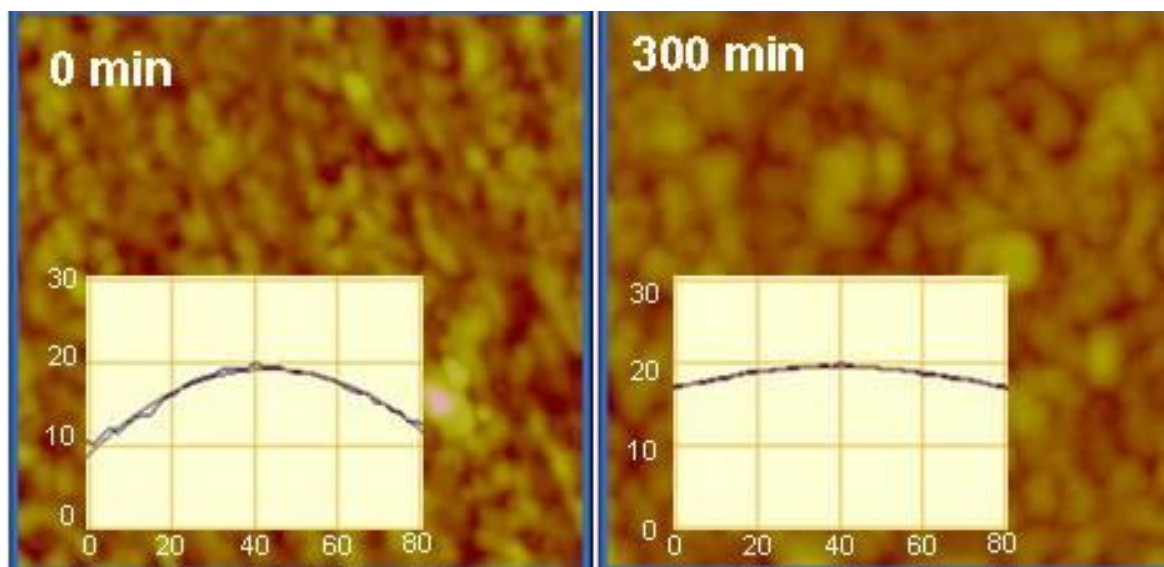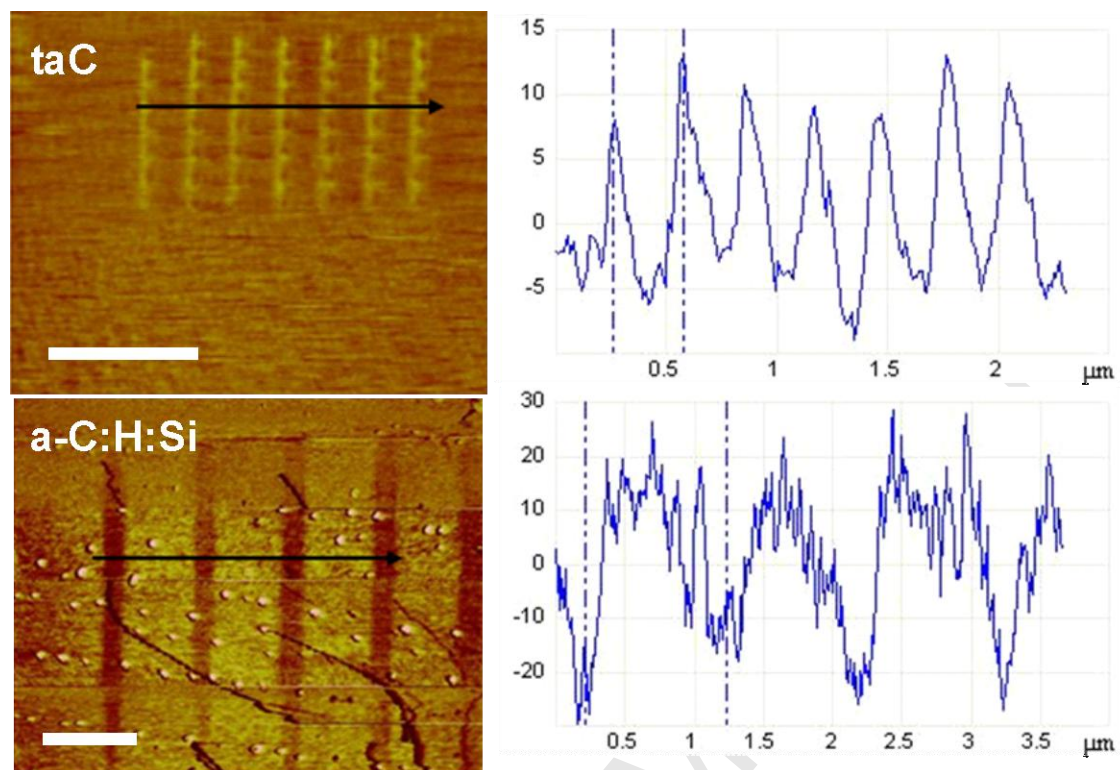
9

Figure 1

Figure 2

Figure 3

12

Figure 4

Figure 5

Figure 6

Figure 7

16
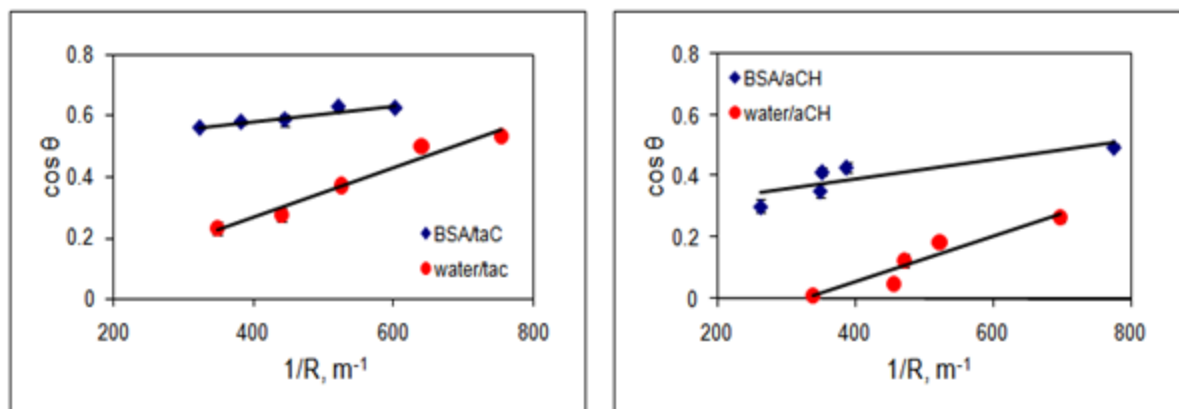
Figure 8

Figure 9

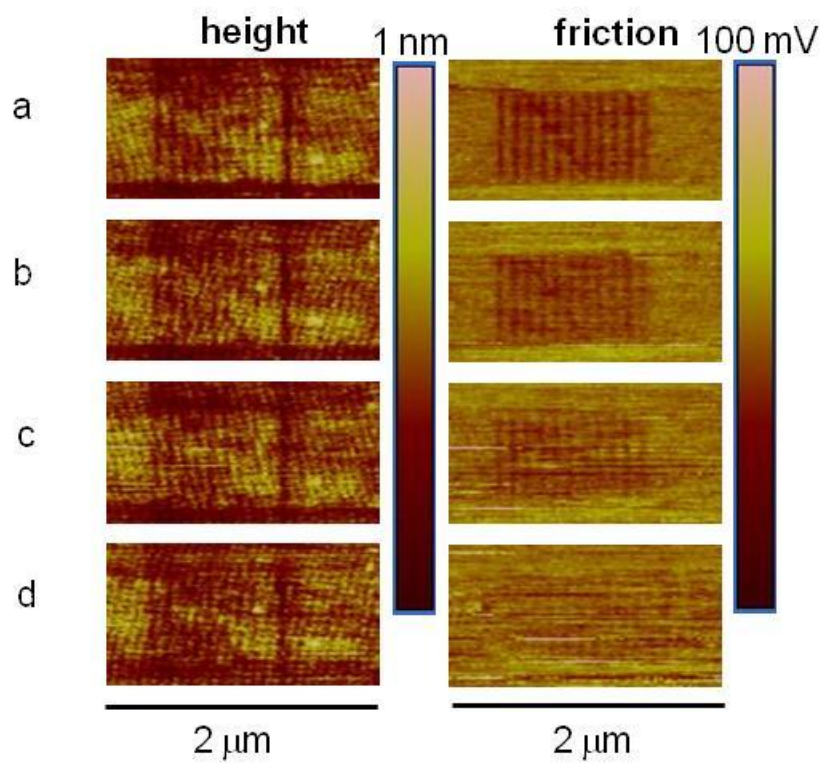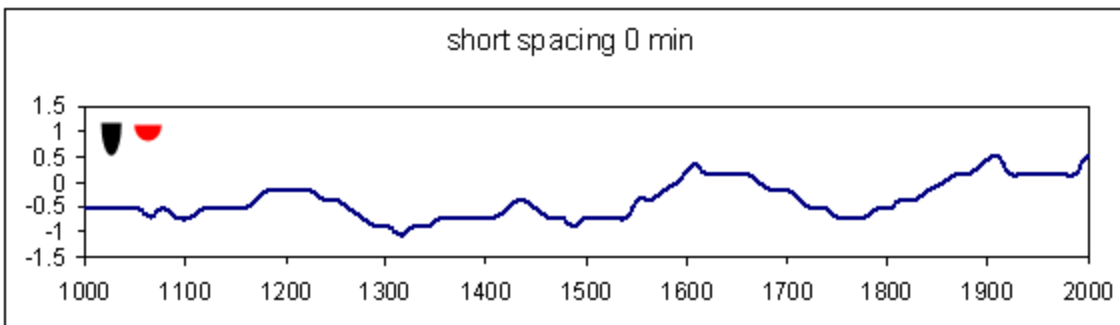**Figure 10**

Figure 11

References

[1] D. C. Cullen, R. Lowe, J Colloid. Inter. Sci. 166 (1994) 102-108.

[2] D. O. Meredith, M. O. Riehle, A. S. G. Curtis, R. G. Richards, J. Mater. Sci. Mater. Med. 18 (2007) 405-413.

[3] F. A. Denis, P. Hanarp, D. S. Sutherland, J. Gold, C. Mustin, P. G. Rouxhet, Y. F. Dufrene, Langmuir 18 (2002) 819-828.

[4] M. Michael Rabe, D. Verdes, Seeger, Adv. Col. Inter. Sci. 162 (2011) 87-106.

[5] P. D. Maguire, J. A. McLaughlin, T. I. T. Okpalugo, P. Lemoine, P. Papakonstantinou, E. T. McAdams, M. Needham, A. A. Ogwu, M. Ball, G. A. Abbas, Diam. Relat. Mat. 14 (2005) 1277–1288.

[6] H. L. Zhou, W. Shi, J. Chin. J. Anal. Chem. 37 (2009) 884–887.

[7] P. Dejardin, Proteins at solid-liquid interfaces, Springer-Verlag, Berlin Heidelberg, 2006, pp. 134.

[8] P. Somasundaran, Encyclopedia of Surface and Colloid Science, second ed., Taylor & Francis, 2006, pp. 5242.

[9] J. F. Zhao, P. Lemoine, Z. H. Liu, J. P. Quinn, P. Maguire, J. A. McLaughlin, Diam. Relat. Mater. 10 (2001) 1070-1075.

[10] P. Papakonstantinou, J. F. Zhao, P. Lemoine, E. T. McAdams, J. A. McLaughlin, Diam. Relat. Mater. 11 (2002) 1074-1080.

[11] NanoInk Inc., private communication.

[12] J. E. Sader, J. W. M. Chon, P. Mulvaney, Rev. Sci. Instrum., 70 (1999) 3967.

[13] B. Pankaj, P. B. Agarwal, A. Kumar, R. Saravanan, A. K. Sharma, C. Shekhar, Thin Sol. Films, 519 (2010) 1025-1027.

[14] J. S. Villarrubia, J. Res. Natl. Inst. Stand. Technol. 102 (1997) 425-454.

[15] B. K. Tay, D. Sheeja, S. P. Lau, J. X. Guo, Diam. Relat. Mater. 12 (2003) 2072–2076.

[16] A. Zebda, H. Sabbah, S. A. Girard, F. Solal, C. Godet, Appl. Surf. Sci. 254 (2008) 4980-4991.

[17] J. Hu, S. Li, B. Liu, J. Biochem. Eng. 23 (2005) 259–263.

[18] D. R. Absolom, C. J. Van Oss, W. Zingg, A. W. Neumann, Biochim. Biophys. Acta. 670 (1981) 74-8.

[19] A. A. Ogwu, T. I. T. Okpalugo, N. Ali, P. D. Maguire, J. A. D. McLaughlin, J. Biomed. Mat. Res. B 85 (*2008*) 105-113.

[20] R. K. Roy, H. W. Choi, J. W. Yi, M. W. Moon, K. R. Lee, D. K. Han, J. H. Shin, A. Kamijo, T. Hasebe,

21

Acta Biomaterialia 5 (2009) 249-256.

[21] D. Li, Coll. Surfaces A: Physicochem. Eng. Asp. 116 (1996) 1-23.

[22] J. A. D. Feijter, A. Vrij, J. Electroanal. Chem. 37 (1972) 9.

[23] P. K. Yadav, P. Lemoine, in preparation.

[24] P. Lemoine, J. McLaughlin, Thin Solid Films 339 (1999) 258-264.

[25] P. Lemoine, J. P. Quinn, P. D. Maguire, J. F. Zhao, J. A. D. McLaughlin, Appl. Surf. Sci. 253 (1997) 6165-6175.

[26] K. J. Wahl, S. A. S. Asif, J. A. Greenwood, K. L. Johynson, J. Coll. Inter. Sci ., 296 (2006) 178-188.

[27] S. J. McClellan, E. I. Franses, Colloid Surfaces A, 260 (2005) 265–275.

[28] M. J. Yaszemski, Tissue Engineering and Novel Delivery Systems, M. Dekker Inc., 2004, pp. 565.

[29] H. Mingyan, A. S. Blum, D. E. Aston, C. Buenviaje, R. M. Overneya, R. Luginbuhl, J. Chem. Phys. 114 (2001) 1355-1360.

22
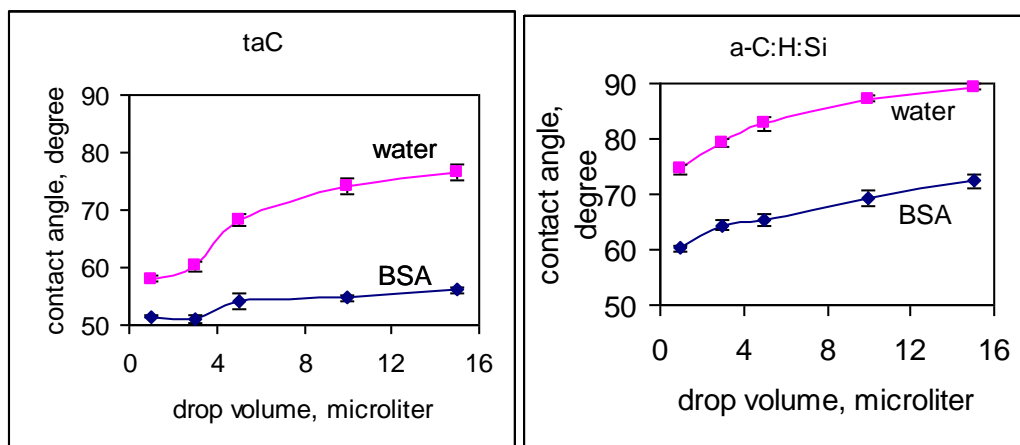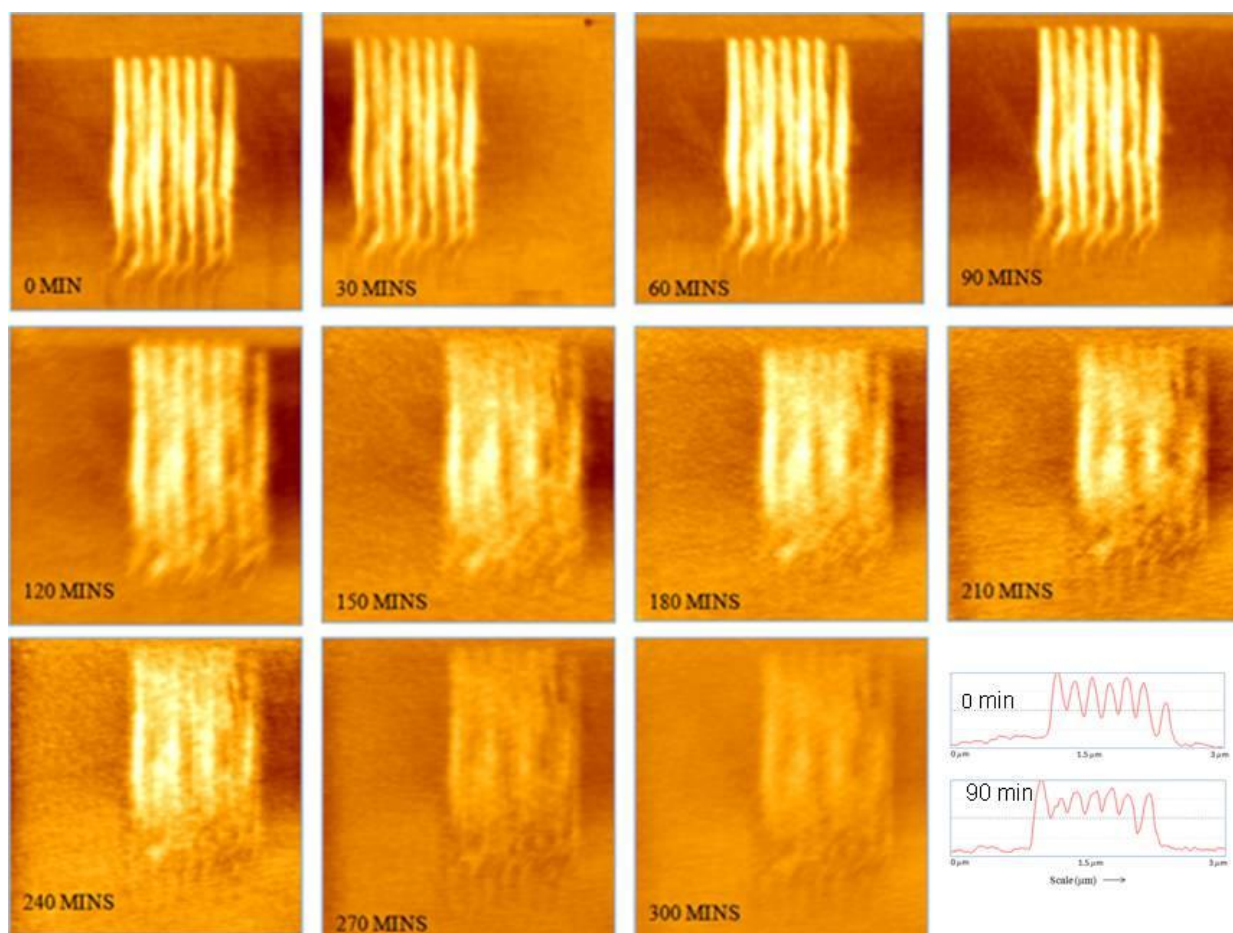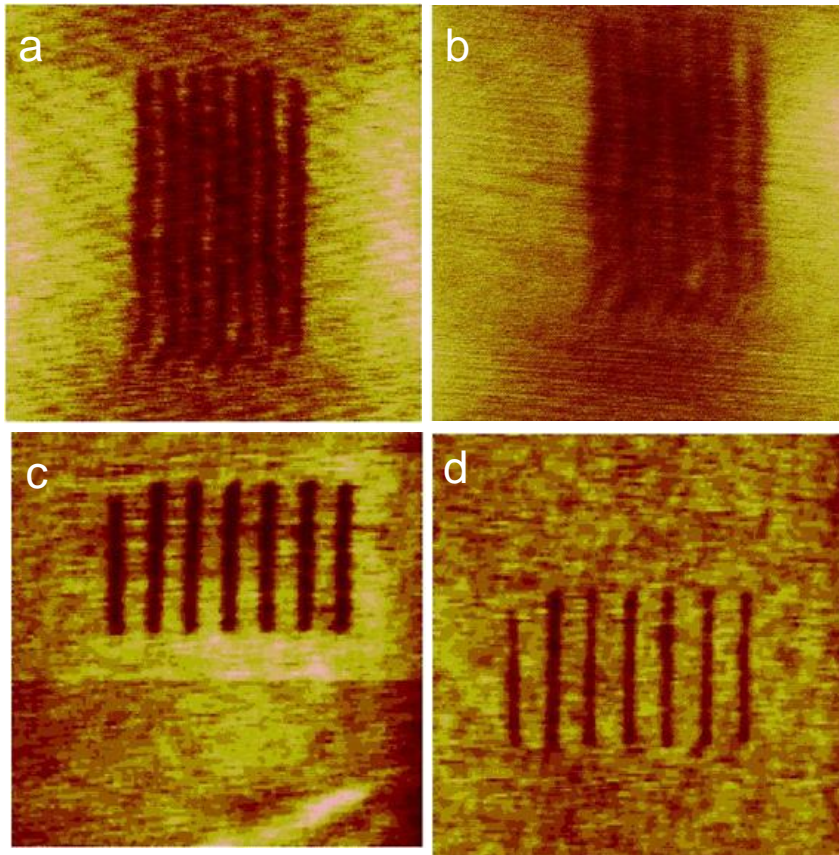
Figure 1

Figure 2

Figure 3

Figure 4

Figure 5

Figure 6

Figure 7

Figure 8

Figure 9

Figure 10

Figure 11